

Case History

Crosswell seismic imaging for deep gas reservoir characterization

Gang Yu¹, Bruce Marion², Brad Bryans², Pedro Carrillo², Guo Wankui³, Pang Yanming⁴, and Kong Fanzhong⁴

ABSTRACT

A gas discovery in the Shengping area of the Daqing Oilfield in China was made recently in a large-scale volcanic depositional environment. Because gas in the heterogeneities of formations broken by tectonic activity and localized volcanic eruptions is not common, researchers sought a more detailed reservoir characterization before developing the field. Crosswell seismic data were used to augment existing 3D surface seismic, log, and core data. This provided data at five times the resolution of the surface seismic data to bridge the gap in resolution between surface seismic and well data. Crosswell seismic data were acquired in two wells, 832 m apart, and processed to provide images of reflectivity, velocity, and formation properties from sections produced by amplitude-versus-angle (AVA) inversion. The state of the art in crosswell seismic is summarized briefly, reviewing progress in data acquisition and data processing over several decades of crosswell technology development. A detailed description of the data acquisition and data processing applied to the data from the Shengping area is also given. An integrated interpretation of the crosswell images with the surface seismic and log data was used to produce a more detailed geologic model. The enhanced geologic model is being used to plan strategic development of the reservoir and to evaluate possible infill well locations.

The Shengping area, part of the Songliao Basin, has deep Shahezhi and Huoshiling dark mudstones and coal seams as a main source of gas. Gas production zones are located in the Yingcheng volcanic and glutenite formations. The Yingcheng formation is the result of large-scale volcanic deposition. Core analysis shows that the volcanic gas-reservoir interval has fracture zones and open pores. The gas zones are shown in the logs of Figure 1 in addition to the rock types from 2400 m to total depth (TD). The volcanic reservoir has fracture zones, melt pores, shrinkage joints, and other features that contribute to significant heterogeneity in the reservoir. The relatively low-resolution surface-seismic data in Figure 2 (with an upper frequency of about 50 Hz) makes mapping the detailed reservoir structure and its lateral extent very difficult. From analysis of well logs, the reservoir zones are typically 3–5 m thick, well below the resolution of surface seismic data.

Researchers selected crosswell seismic data to provide higher resolution reservoir description, combined with existing 3D surface seismic, VSP, and log data. Crosswell seismic data was chosen with these specific objectives: (1) map lateral changes and extent of reservoir formation between wells, (2) provide critical reservoir-distribution information to optimize the gas-field development plan, and (3) select infill well locations between the existing exploration and evaluation wells. As a location where infill well opportunities might exist, researchers selected the area around the SS-2-17 and SSG-2 wells for reservoir characterization (see Figure 3). Their goal was an integrated interpretation using all available data to enhance the geologic model of the area.

INTRODUCTION

A new deeper gas field was discovered recently near the outer boundary of the prolific Daqing Oilfield. The newly discovered gas field is located in a large-scale volcanic depositional environment.

REVIEW OF THE STATE OF THE ART IN CROSSWELL SEISMIC

Crosswell seismic technology has been under development since the early 1980s with many research groups inside major E & P companies involved in early experiments (Lines et al., 1993). Initially re-

Manuscript received by the Editor 3 June 2008; published online 5 November 2008.

¹KMS Technologies, Houston, Texas, U.S.A. E-mail: gang@kmstechnologies.com.

²Z-Seis Corporation, Houston, Texas, U.S.A. E-mail: bmarion@z-seis.com; bbryans@z-seis.com; pcarrillo@z-seis.com.

³Deceased.

⁴Daqing Oilfield E & D Institute, P. R. China. E-mail: pangyanming@petrochina.com.cn; kongfzh@sina.com.

© 2008 Society of Exploration Geophysicists. All rights reserved.

searchers focused on tomographic inversion of direct-path travel-time data to produce velocity images. Early source technology was limited in reach to about 100 m between wells, and wells had to extend past the reservoir interval for the tomographic image to have full coverage. During the 1990s, researchers at Stanford University demonstrated reflection imaging using crosswell seismic data (Harris et al., 1995). Over the past 15 years, crosswell seismic technology advances have occurred primarily in the area of improved down-hole sources and enhanced data processing and analysis methods. A recent search of the online SEG database revealed 257 references to crosswell seismic methods. The Daqing gas-field study is one of the most challenging large-scale projects in China to consider crosswell data acquisition.

The benefits of advanced crosswell seismic technology include:

- Improved understanding of the reservoir with impact on all phases of exploitation and recovery.

- Increased distance between wells.
- Improved efficiency and lower cost.
- More robust processing and interpretation.
- Reduced impact on production operations.

Innovative technologies introduced in the past decade include:

Acquisition

- More powerful sources providing for operation up to 1 km between wells (Antonelli et al., 2004).
- Multilevel receivers for enhanced efficiency (Li and Majer, 2003).

Data processing

- Fully 3D imaging framework (Washbourne et al., 2002b).
- TI anisotropy estimated in inversion and applied in ray tracing (Jervis et al., 2000).
 - Pre-stack migration (Byun et al., 2001).
 - Reflection tomography — no missing coverage at TD (Washbourne et al., 2002a).
 - Crosswell amplitude decomposition and AVA inversion (as described here).
 - Difference tomography for time-lapse applications (Bryans, 2004).
 - Attenuation tomography (Carrillo et al., 2007).

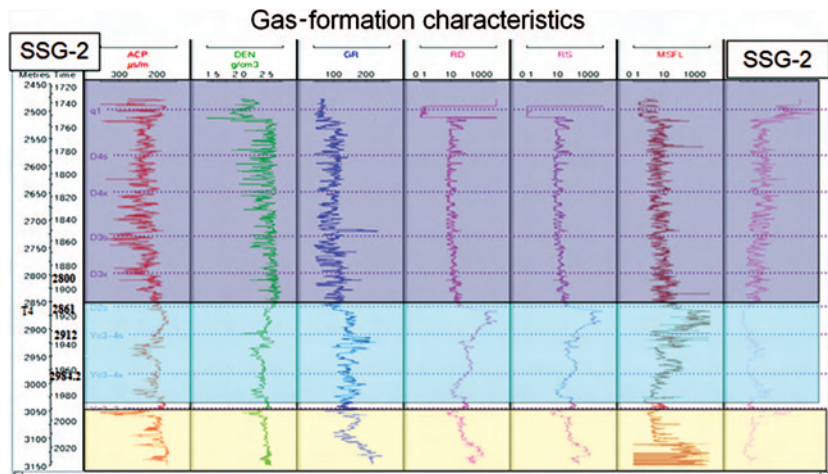


Figure 1. Gas-formation characteristics in well logs from well SSG-2. Rock types from 2400 m to TD are listed.

DATA ACQUISITION AND PROCESSING METHODS

Researchers collected data from one crosswell seismic profile (survey between a pair of wells) in the Shengping area of the Daqing Oilfield during September 2005. The crosswell seismic piezoelectric source was deployed in the SS-2-17 well (Figure 3). A multilevel, high-frequency, down-hole hydrophone-receiver system was deployed in the SSG-2 well (Figure 3). The distance between the two wells at the surface was 832 m, which was a well separation greater than most previous crosswell surveys reported to date in China. The objective imaging zone was from 2500–3400 m. During data acquisition, the down-hole seismic source was positioned at depths between 2154–3093 m, and the downhole seismic receiver was positioned at depths from 2229–3366 m. Both source spacing and receiver-level spacing were 3 m, providing a finely sampled data set. A high degree of redundancy (fold) resulted for crosswell seismic tomographic inversion and reflection imaging. In addition, the fine sampling allowed multichannel wavefield separation filtering of the time-domain crosswell seismic data. Because well spacing was very large compared with normal crosswell seismic profiles, researchers used a configured downhole seismic source to increase the energy. Two piezoelectric sources operated simultaneously in the source well, resulting in a longer source with twice the

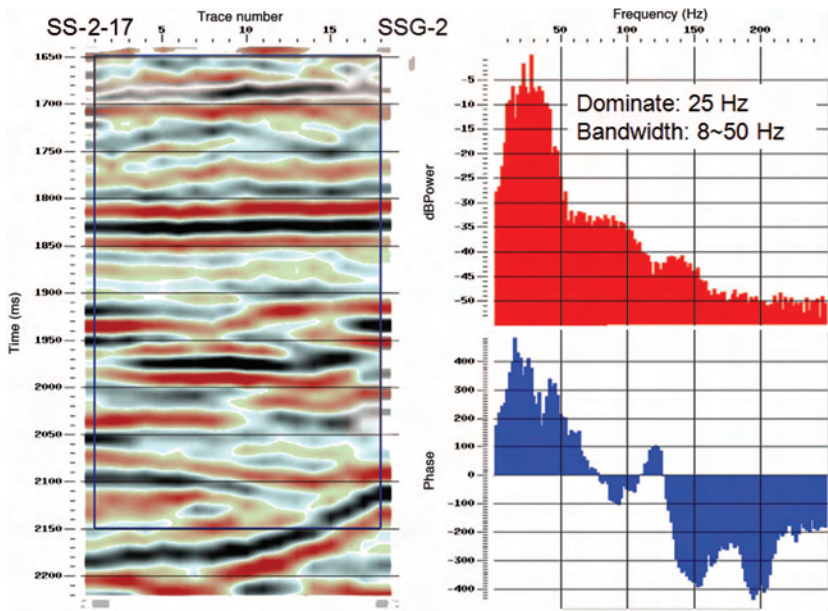


Figure 2. The relatively low-resolution surface seismic data between SS-2-17 and SSG-2 (left), with an upper frequency of about 50 Hz (right), makes mapping of the reservoir structure and lateral extent very difficult.

output. The source sweep frequency range was from 100 Hz–1000 Hz. This source configuration is estimated to increase energy by 6 dB and improve the signal-to-noise ratio.

Operational challenges included high noise levels in the source and receiver wells. The major noise source was from gas movement between different zones behind the casing. Researchers applied *f-k* filtering to the time-domain data in the field to enhance the direct arrival and reflected wavefields. See Figure 4 for examples of common source-and-receiver gathers (raw data), where high-amplitude reflections are identified with black arrows. There were 81,330 traces of crosswell seismic data acquired successfully for the profile separated by 832 m.

Processing of the crosswell seismic data set is conducted in two major phases: tomographic inversion to produce an image of velocity between the two wells and a velocity model, and reflection imaging. Figures 5 and 6 outline the steps in each processing phase. In this study, researchers used AVA gathers from the reflection-imaging process to invert for velocity and density sections between the wells to enable better interpretation of formation properties between the two wells. The inversion used reflectivity at each offset location between the wells as a function of angle as the input to the AVA inversion process. Incidence angles in the crosswell data as measured from the vertical are in the range of approximately 40° to more than 85°, a greater-than-typical range in surface seismic AVO inversion. Figure 7 illustrates an example of a crosswell AVA gather from an offset of 192.5 m from the receiver well.

Based on the large vertical zone of interest for crosswell seismic imaging, reflection seismic data from above the source and receiver positions (downgoing reflections) were used in addition to reflection data from below the source and receiver positions (upgoing reflections). This process reduces the number of levels to be acquired to

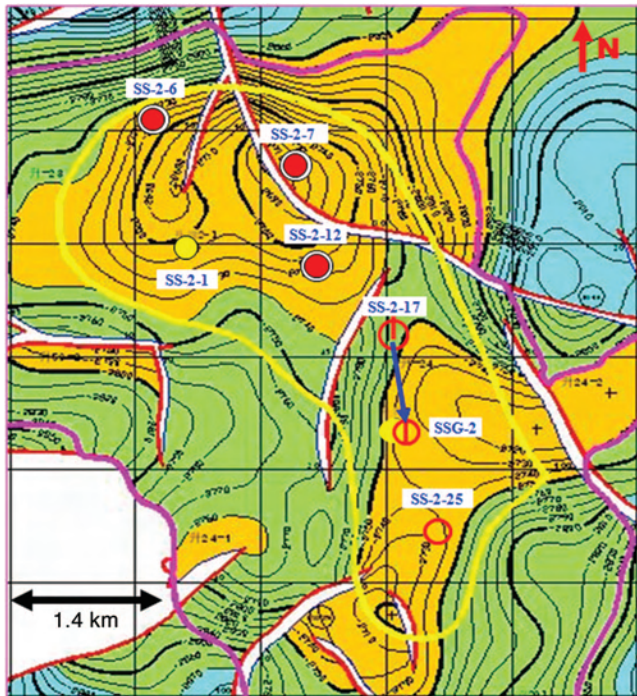


Figure 3. The area around the SS-2-17 and SSG-2 wells was selected for characterization using the crosswell seismic method and as a location where infill well opportunities might exist.

cover a tall zone of interest (D’Agosto et al., 2006). Researchers used similar data-processing flows for both upgoing and downgoing reflection images, with the exception of the up/down reflection separation step of the wavefield separation processing.

Data processing and velocity tomography

In the crosswell seismic tomographic processing sequence, each trace was first noise-edited with diversity stacking and crosscorrelated with the pilot signal (sweep). Then the correlated data were stacked to generate a 3-m depth increment in both the source and receiver well. Crosswell data often contain tube waves of high amplitude. Tube waves are strong signals that travel within the well and can affect the energy content of reflections. Tube waves were identified in common source-and-receiver gathers. As a result of tube-wave noise, both coherent and random in the data, a reject filter was applied in two crosswell domains: common-receiver gather (CRG) and common-source gather (CSG). A 17-point median filter (time-domain wavefield) was designed to reject the upgoing and downgoing tube waves. In addition the data were zero-phase, band-pass filtered (time domain) with an Ormsby filter using corner frequencies (225 Hz ~ 250 Hz ~ 750 Hz ~ 850 Hz) prior to first-arrival time picking.

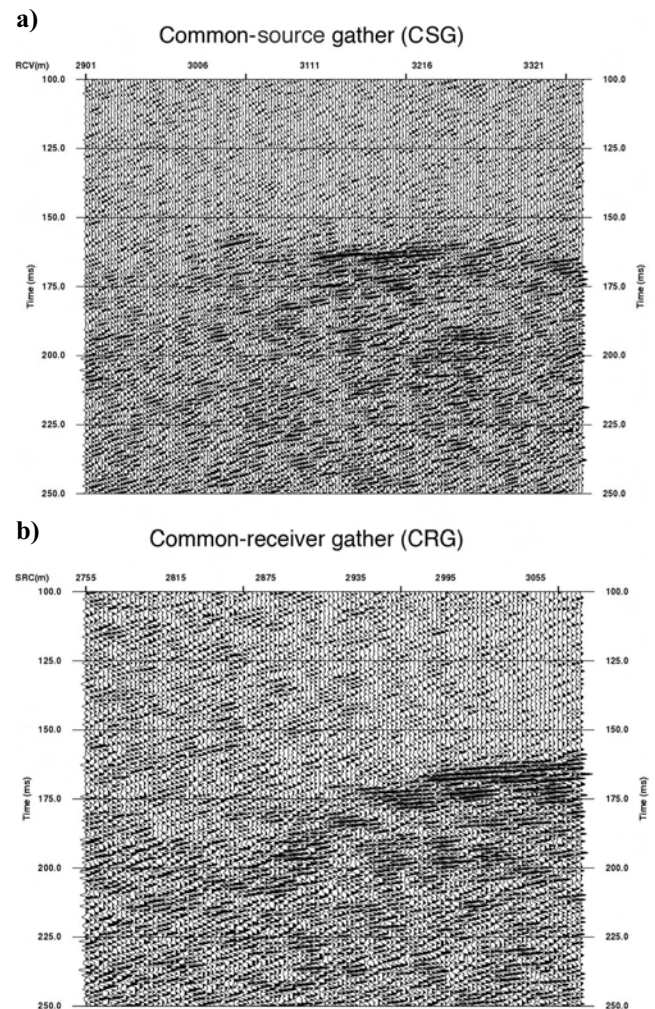


Figure 4. Example of raw data. (a) Common-source gather. (b) Common-receiver gather. Arrows indicate events related to reflections.

Then we identified and picked the crosswell seismic P-wave first arrivals in four domains: common-receiver gather (CRG), common-source gather (CSG), common-offset gather (COG) and common-mid-depth gather (CMG). The complexity of the crosswell wavefield sometimes makes it difficult to identify the first arrivals. The four domains allow redundant confirmation of the picks. The P-wave first-arrival pick times were considered as input to the 3D anisotropic traveltime inversion. The crosswell seismic 3D anisotropic traveltime-tomography algorithm (Washbourne et al., 2002b) produces an image of seismic velocity between wells using the nonlinear continuation strategy of Bube and Langan (1999).

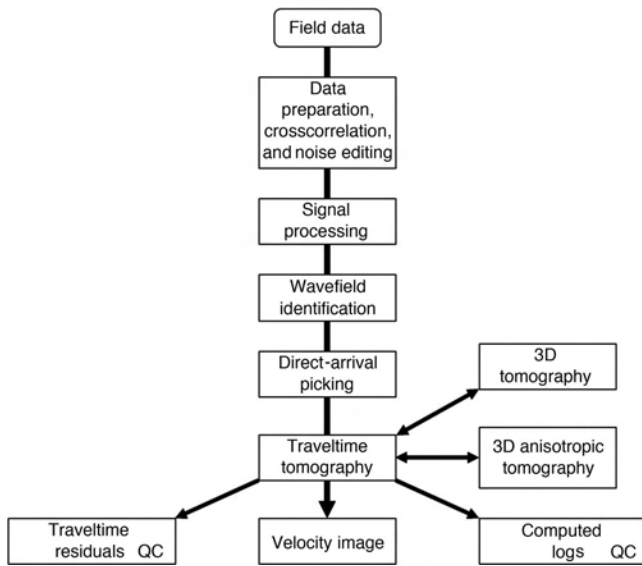


Figure 5. Crosswell seismic data tomographic-inversion processing steps and flowchart.

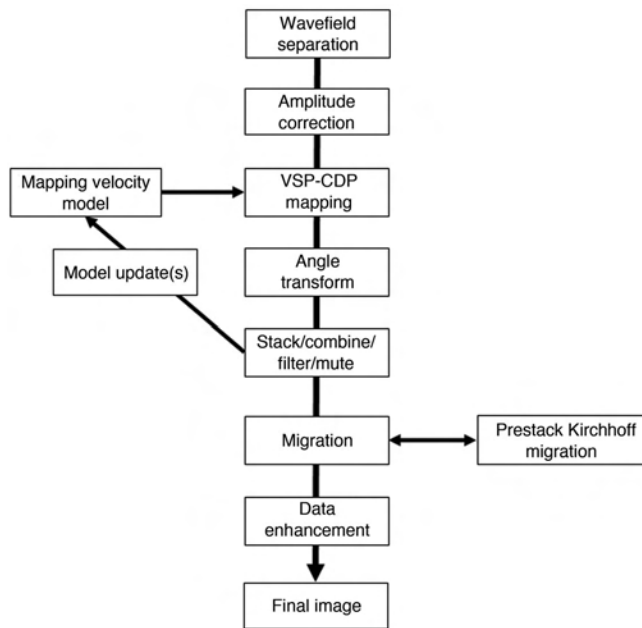


Figure 6. Crosswell seismic data reflection-imaging processing steps and flowchart.

Coherent wave modes in the time-domain wavefield can contribute noise to the final stacked image. These wave modes include compressional direct arrivals, shear direct arrivals and shear reflections. These wave modes are removed through spatial filtering. In this project, unwanted wave modes were attenuated using spatial filters (usually f - k fan or median filters) applied in various crosswell sort domains. Wavefield-separated data were deconvolved with a zero-phase spiking filter.

Reflection amplitudes recorded in crosswell seismic data are affected by several factors that are not related to the reflection coefficient of a reflecting horizon. The goal of amplitude normalization is to correct the amplitudes of time-domain data before mapping. Here the amplitude normalization used to balance amplitude was computed trace-by-trace over the time window -10 ms to $+100$ ms around the P-wave first-arrival time.

Reflection imaging

The wavefield-separated crosswell seismic data in the study were VSP-CDP depth mapped, as in offset-VSP data processing, using the velocity model from the crosswell seismic traveltime inversion. Researchers carried out a post-map migration (Byun et al., 2001) on the VSP-CDP-mapped data volume to collapse diffractions and produce the final crosswell seismic reflection image. Because there is a wide range of incidence angles present in a crosswell seismic data set and the wavelet and reflection character change with incidence angle, the angle-transformed AVA data volume is another natural domain for data analysis. Angle muting was used in this case to select angles that

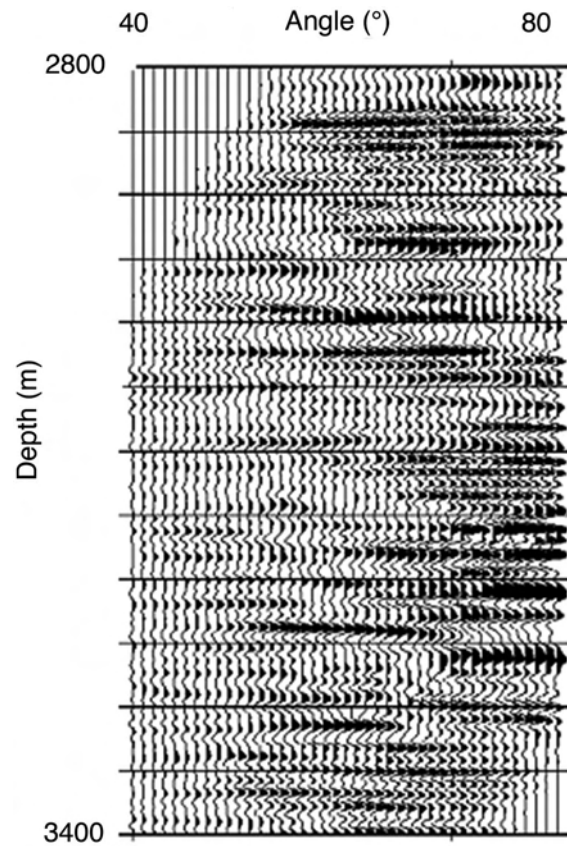


Figure 7. Crosswell AVA gather from an offset of 192.5 m from the receiver well.

maintain adequate SNR while best approximating the vertical incidence response. Following stacking of the AVA data volume, we applied a depth-domain bandpass filter and short mix across traces to improve the SNR in the stacked final reflection image.

AVA reflectivity inversion

We applied amplitude compensation to the crosswell data to preserve reflectivity amplitudes in the AVA gathers. Direct-arrival amplitudes were used as input to an amplitude decomposition that describes amplitude as made up of source, receiver, and absolute offset (vertical offset = source depth – receiver depth) terms. The source-and-receiver terms take into account near-wellbore effects such as formation impedance, the interfaces between fluid and casing, fluid and cement, and cement and casing, and equipment effects like depth-dependent source amplitude, or channel-to-channel gain and sensitivity differences in the receiver system. The absolute-offset term accounts for angle dependence in the source-and-receiver radiation patterns in addition to propagation effects such as transmission coefficients, distance, and attenuation. We derived petrophysical properties using AVA inversion based on linearized approximations to Zoeppritz equations (D’Agosto et al., 2008). Researchers obtained dV_p/V_p , dV_s/V_s , and $d\rho/\rho$ with a linear, least-squares inversion approach. Then the low-frequency trend was added for the AVA inversion output (V_p , V_s) and density inversions. The low-frequency trend for V_p was derived from the crosswell seismic velocity image from tomographic inversion. Resulting V_p and density values were combined to generate an acoustic impedance section.

Crosswell seismic images, interpretation and integration

Figure 8 depicts the final compressional velocity image from the tomographic inversion result. Well-log data (gamma ray, acoustic, and density) and tomographic velocity value from the edges of the velocity profile are plotted on both sides of the velocity image to assist in correlating and validating tomographic inversion results. Researchers employed this crosswell seismic velocity image as the velocity model for reflection imaging and as the low-frequency trend used with the AVA inversion output to produce a final V_p section.

Downgoing reflections have a polarity opposite to upgoing reflections because of changes in the reflection coefficients during the incidence process of a wave. The downgoing reflection image was polarity flipped and then combined with the upgoing reflection section in a final image. Figure 9 illustrates the combined upgoing and

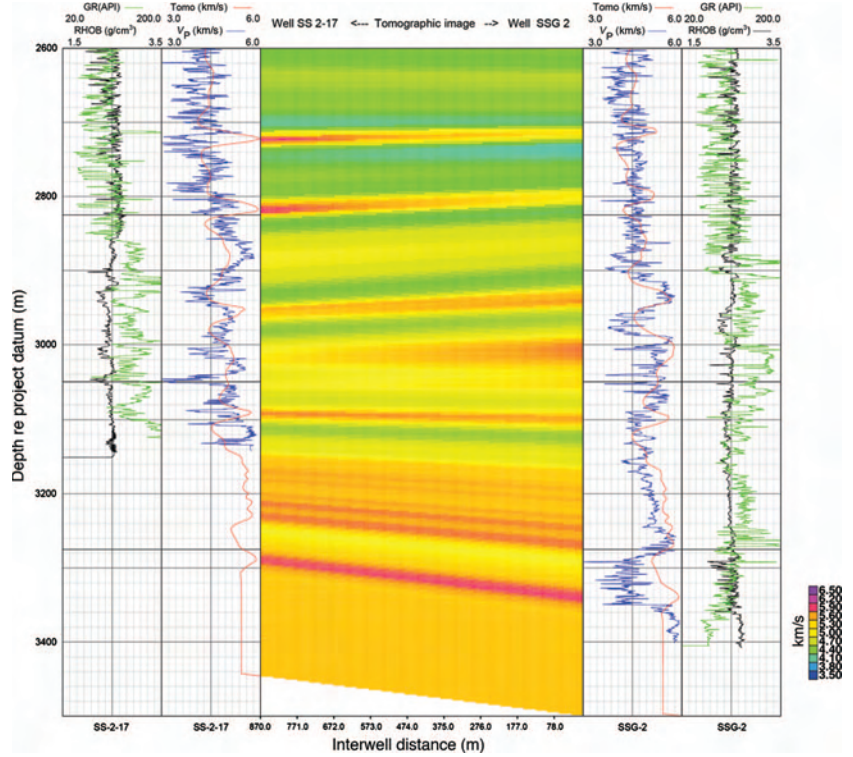


Figure 8. Final compressional velocity image from the tomographic-inverted velocity model. Tomogram velocity values and well-log data for source (left) and receiver (right) wells are depicted.

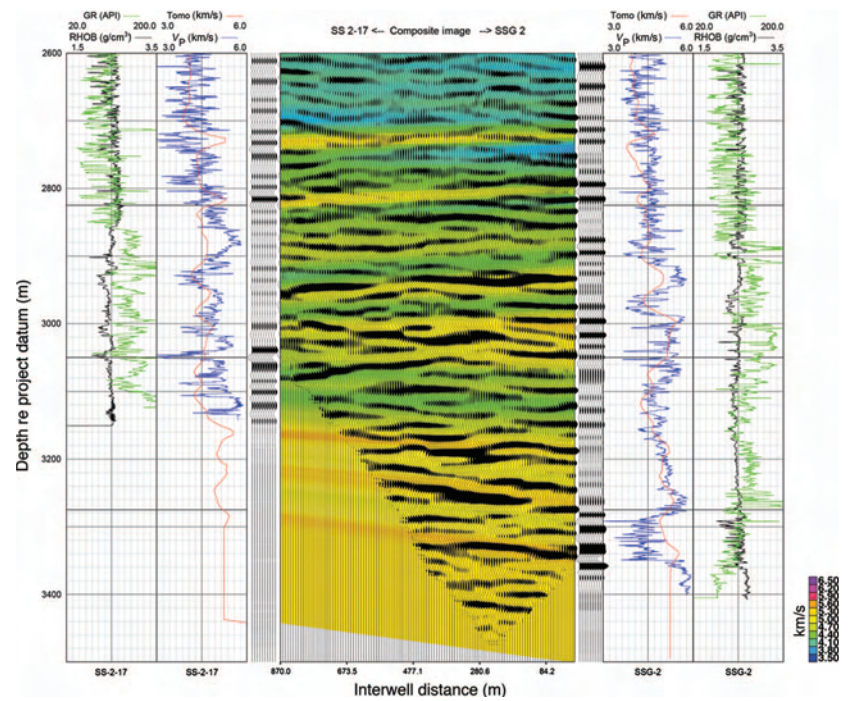


Figure 9. Final composite combined-reflection image and tomographic-inverted velocity model. Well-log data, tomogram velocity values, and synthetic seismograms for source (left) and receiver (right) wells are illustrated. Note that synthetic seismograms match the reflection image closely.

downgoing reflection image, overlaid on the final velocity image from tomographic inversion. In addition to well-log data and tomographic velocities logs, synthetic seismograms were plotted and correlated with the major seismic events present in the reflection image. In comparison with the 50-Hz surface seismic data (Figure 10), the crosswell seismic profile has at least five times the resolution of the surface seismic data and reveals the detailed subseismic-scale structure with a resolution of 3–5 m.

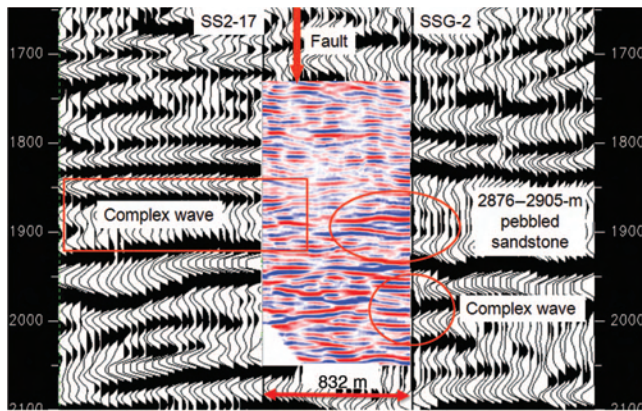


Figure 10. Comparison of the 50-Hz surface seismic data with crosswell seismic data shows that the profile has at least five times the resolution of surface seismic data and reveals the detailed subseismic-scale structure with a resolution of 3 to 5 m.

Daqing Oilfield interpreters used the final crosswell seismic reflection image to map the detailed reservoir structure between the two wells (Figure 11). Faults that are expressed subtly in the surface seismic data are quite clear in the crosswell images, and an additional scale of reservoir data is available in the crosswell structural image to enhance the geologic model. AVA inversion results were used to produce an impedance section (Figure 12) and a density section (Figure 13). From the well positions located at the edges of the impedance and density images obtained, values were extracted and plotted along with the rest of the well-log data. These data were used to derive additional interpretive displays discussed below.

Instantaneous amplitude, or reflection strength, is the square root of the total energy of the seismic signal at an instant of time. Then reflection strength can be thought of as amplitude independent of phase. It is the envelope of the seismic trace. Therefore reflection strength is always positive and always in the same order of magnitude as the recorded trace data. Reflection strength is an effective tool to identify bright and dim spots. It provides information about contrasts in acoustic impedance. Lateral changes in reflection strength are often associated with major lithologic changes or with hydrocarbon accumulations. Gas reservoirs, in particular, appear frequently as high-amplitude “bright spot” reflections.

The reflection-strength AC component (Figure 14) was derived based on crosswell seismic reflectivity data. The reflection-strength AC component is the amplitude envelope (reflection strength) with the DC component removed. It is suggested that such a display would make the locations of energy maxima more obvious in the seismic section. The reflection-strength AC component has essen-

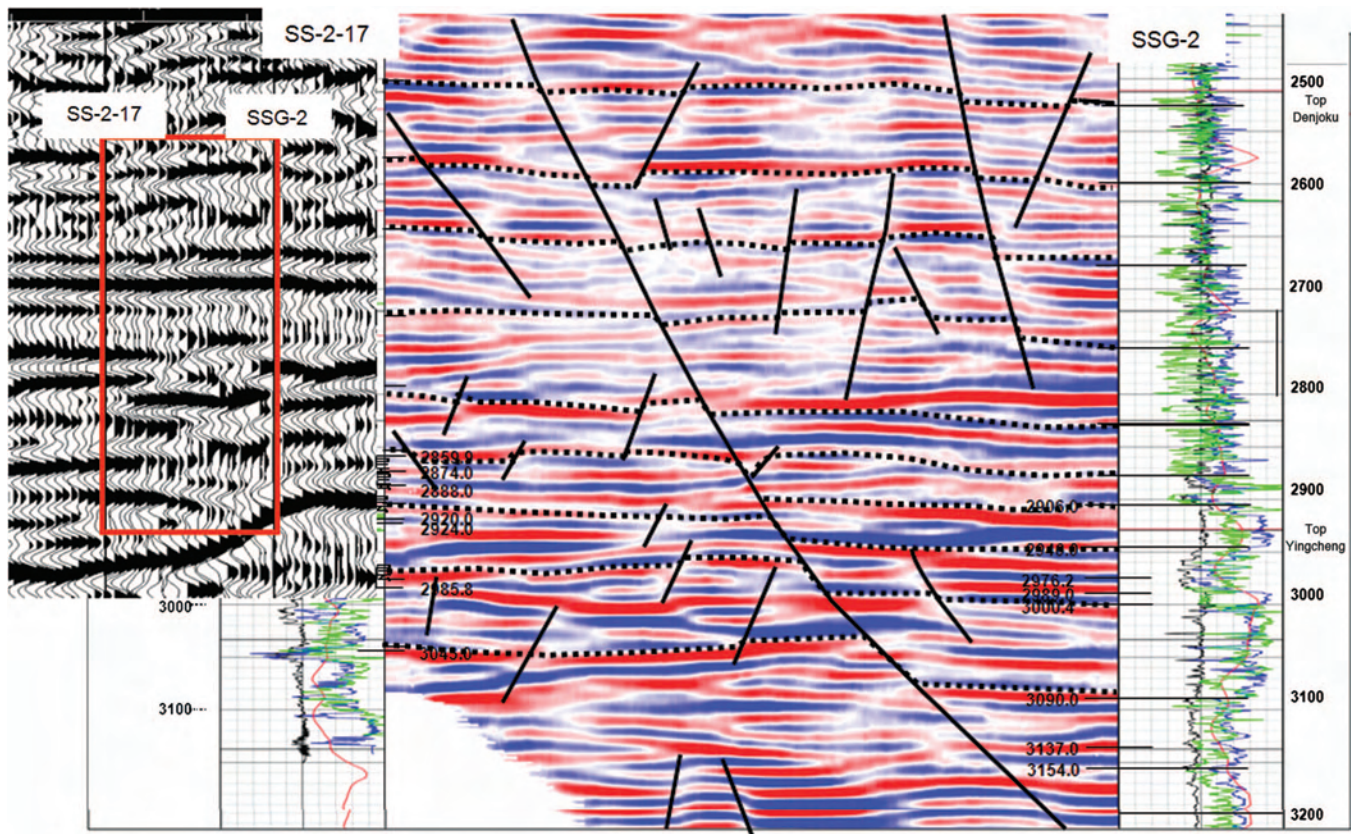


Figure 11. Structure and fault interpretation from the final reflection image between the two wells. Faults that are expressed subtly at best in the surface seismic data are quite clear in the crosswell images.

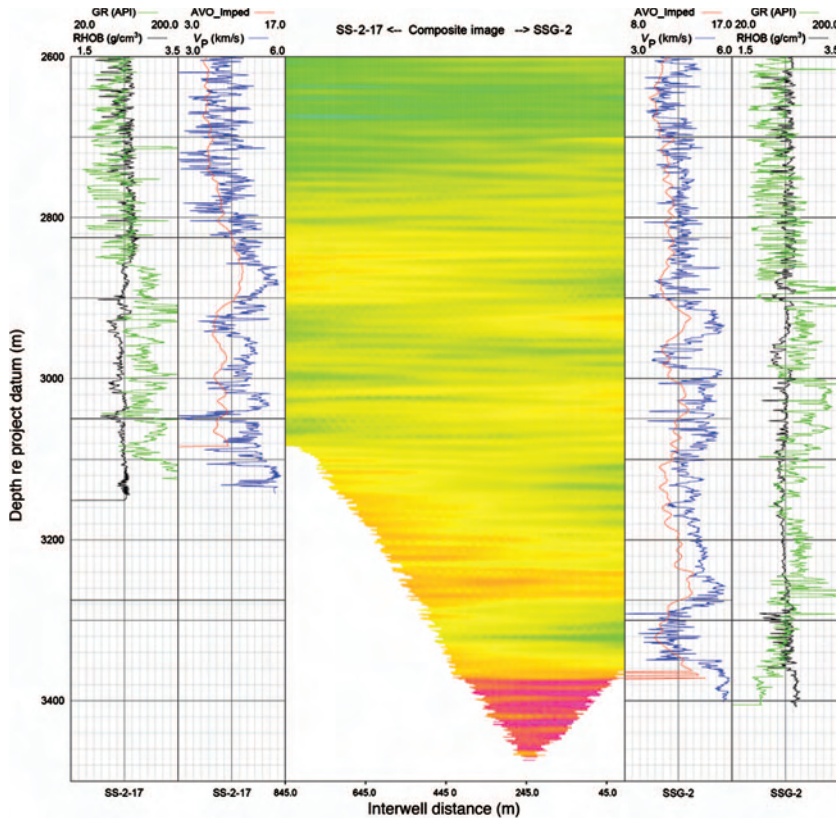


Figure 12. Final AVA- V_p inverted acoustic-impedance image. Well-log information and AVA- V_p inverted acoustic-impedance values at wells are plotted on both sides of the impedance image. Note the correlation between impedance log (red), sonic velocity log (blue), and density log (black) between 2600–3100 m (well SS-2-17) and 2600–3300 m (well SSG-2).

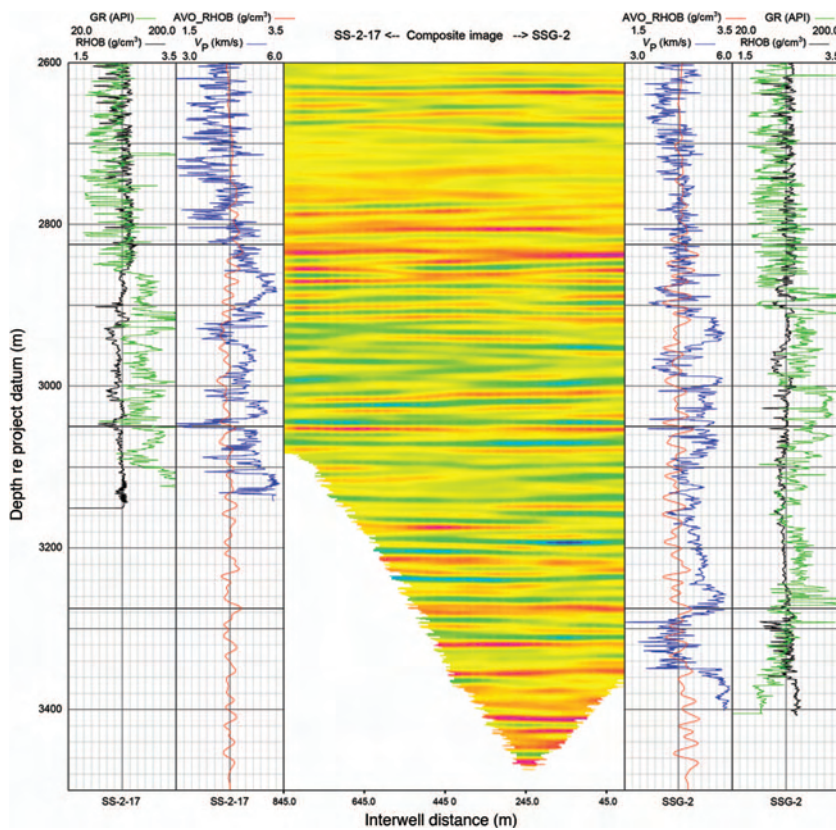


Figure 13. Final AVA-inverted density image. For low-frequency content, inversion results (red) show correlation with the density log (black) between 2600–3100 m (well SS-2-17) and 2600–3000 m (well SSG-2).

tially the same uses as reflection strength, but because its data has both positive and negative values, it can be analyzed with standard color maps and subjected to trace mixing or other data-enhancement processes. Reflection-strength data, because it is only positive, is not suitable for many types of analysis and processing.

Researchers found reflection-strength AC-component data to be an indicator of volcanic formations based on well control. In addition, this attribute was used to map lateral variations of lithology formation. The analysis showed that the Glutinite in SS-2-17 (2740 ~ 2862 m) and pebbled sandstone in SSG-2 (2876 ~ 2900 m) have reflection-intensity changes, but they are weaker than in volcanic rocks. Low-impedance zones were identified (see Figure 15). The impedance profile is derived from crosswell seismic data with interpretation of gas zones based on the presence of low impedance. Using the impedance profile, we can see two low-impedance zones (red and purple) in the YC3-4 group and one low-impedance zone in the YC3-3 group that are associated with the gas reservoir. One low-impedance zone (volcanic deposit facies) in the YC4 group matches the

known gas zone in the well SSG-2. An integrated interpretation produced the final integrated reservoir-scale geologic model in Figure 16. This detailed subseismic geologic model has at least five times the resolution of the geologic model produced with previously available surface seismic data. In addition to enhancing what is known of the reservoir, the more detailed information is used to evaluate infill well locations for gas-field development.

After the integration of surface seismic data, crosswell seismic data, log-data interpretation, and different crosswell seismic attribute analyses, the final integrated gas-reservoir evaluation profile was created (see Figure 17). During the final integration study phase, the crosswell seismic-derived attributes of instantaneous frequency, instantaneous phase, reflection-intensity AC component, seismic impedance, interval velocity, density, calculated gamma, inverted Poisson's ratio, spectral decomposition, and coherence were derived and analyzed with the reservoir-scale structural interpretation to map and describe the gas reservoir distribution between two wells.

Figure 14. Researchers used the reflection-strength AC component to analyze the quality of amplitude anomaly and to map the lateral variations of lithology formation. The reflection-strength AC component is the deviation after removal of the average value (DC component) of reflection strength.

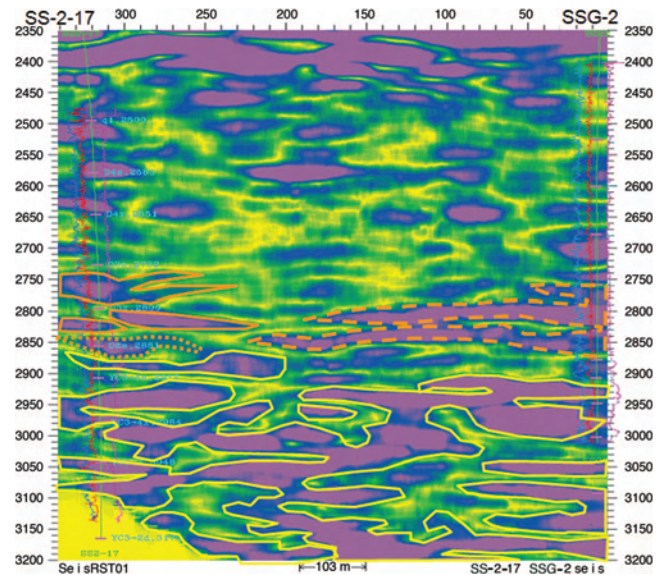
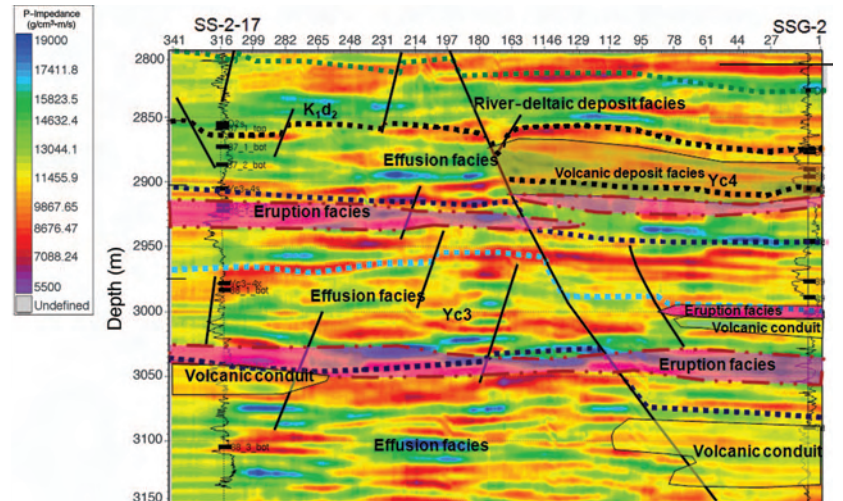


Figure 15. The impedance profile was used for reservoir prediction. Two low-impedance zones (red or purple) in the YC3-4 group and one low-impedance zone in the YC3-3 group were predicted from the impedance profile. One low-impedance zone (volcanic deposit facies) in YC4 group matched the gas zone in the SSG-2 well.



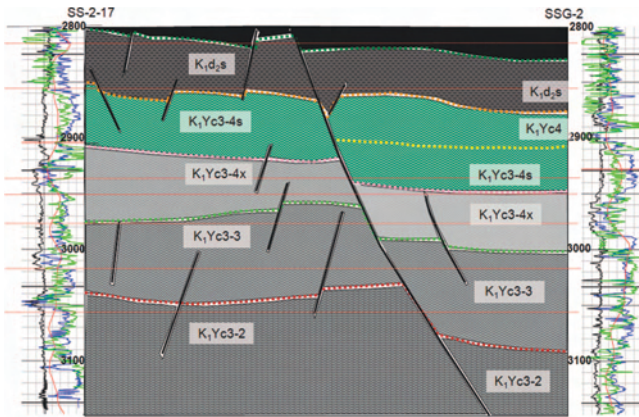


Figure 16. Final integrated interpretation of reservoir-scale geologic-structure profile. Note that well logs — gamma ray (green), density (black), P-wave velocity (blue), and tomogram velocity (red) — follow the geology of the area.

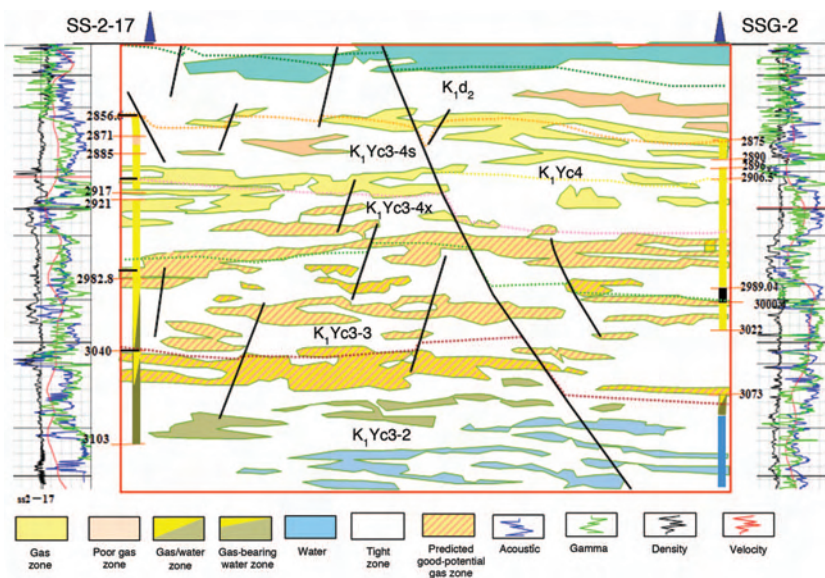


Figure 17. Final integrated interpretation of gas-reservoir distribution and profile evaluation. Gamma ray, density, P-wave velocity, and tomogram velocity logs at wells are shown in green, black, blue, and red, respectively.

CONCLUSION

Based on additional resolution provided by crosswell seismic data in imaging formations between the wells, researchers developed an enhanced geologic model of the Shengping gas field. The crosswell reflection data provided greater detail in reservoir structure between wells, revealing small-scale faulting that was incorporated into the geologic model. AVA inversion of the crosswell data provided new insight into reservoir formation properties. Ties of the inverted impedance to well control allowed imaging of the distribution of gas zones between wells.

Researchers are using the enhanced reservoir model resulting from integrated interpretation of surface seismic data, log-derived information, and crosswell seismic images to plan strategic development of the reservoir and to evaluate possible infill well locations. This study demonstrates the role of crosswell seismic data in providing information to fill the gap between surface seismic and log data.

The successful application of crosswell data from wells separated by over 800 m makes crosswell seismic data a candidate method for integrated reservoir characterization between wells in many oil and gas fields.

ACKNOWLEDGMENTS

This project was made possible by the effort and dedication of many professionals at PetroChina and Daqing Oilfield. We specifically acknowledge the support of Daqing management in facilitating the entire project. We greatly appreciate Daqing Oilfield’s permission to release the data and allow us to publish this study.

REFERENCES

Antonelli, M., F. Miranda, L. Terzi, and G. Valenti, 2004, Integrated crosswell seismic: Case histories in advanced technologies to improve reservoir description: *First Break*, **22**, 49–56.

Bryans, B. W., 2004, Monitoring of SACROC CO₂ flood utilizing crosswell tomography and reflection imaging: West Texas Geological Society Fall Symposium, Expanded Abstracts, 255–256.

Bube, K., and R. Langan, 1999, On a continuation approach for regularization for crosswell tomography: 69th Annual International Meeting, SEG, Expanded Abstracts, 1295–1298.

Byun, J., J. Rector, and T. Nemeth, 2001, Two-step migration approach for crosswell seismic reflection data: 71st Annual International Meeting, SEG, Expanded Abstracts, 1–4.

Carrillo, P., M. Aldana, B. Bryans, and R. Turpening, 2007, Attenuation coefficient tomogram and Q distribution image from crosswell survey in the Northern Reef Trend of Michigan Basin: 77th Annual International Meeting, SEG, Expanded Abstracts, 1252–1255.

D’Agosto, C., M. Antonelli, and F. Miranda, 2006, Enhanced crosswell acquisition efficiency with combined upgoing and downgoing imaging: 76th Annual International Meeting, SEG, Expanded Abstracts, 1–4.

D’Agosto, C., M. Antonelli, F. Miranda, R. Micheli, and M. Salah, 2008, Integrated crosswell seismic inversion — Test on Belayim land data: 70th Annual EAGE Annual Conference and Exhibition, EAGE, Extended Abstracts, 9–12.

Harris, J. M., R. Nolen-Hoeksema, R. T. Langan, M. Van Schaack, S. K. Lazaratos, and J. W. Rector, 1995, High resolution imaging of a west Texas carbonate reservoir: Part 1 — Project summary and interpretation: *Geophysics*, **60**, 667–681.

Jervis, M., C. Addington, J. K. Washbourne, H. Malcotti, M. Capello, and M. Vasquez, 2000, High resolution crosswell reflection imaging in the presence of anisotropy — The Santa Rosa gas field, Eastern Venezuela: 70th

- Annual International Meeting, SEG, Expanded Abstracts, 1631–1635.
- Li, G., and E. Majer, 2003, Coiled tubing deployment makes crosswell seismic surveying successful in horizontal wells: *The Leading Edge*, **22**, 454–458.
- Lines, L. R., M. Miller, H. Tan, R. Chambers, and S. Treitel, 1993, Integrated interpretation of borehole and crosswell data from a west Texas field: *The Leading Edge*, **12**, 13–16.
- Washbourne, J., K. Bube, M. Antonelli, and F. Miranda, 2002a, Crosswell reflection tomography: 72nd Annual International Meeting, SEG, Expanded Abstracts, 874–877.
- Washbourne, J., J. Rector, and K. Bube, 2002b, Crosswell traveltime tomography in three dimensions: *Geophysics*, **67**, 853–871.